www.MaterialsViews.com

ADVANCED
ENERGY
MATERIALS
www.advenergymat.de

COMMUNICATION

High-Areal-Capacity Silicon Electrodes with Low-Cost Silicon Particles Based on Spatial Control of Self-Healing Binder

Zheng Chen, Chao Wang, Jeffrey Lopez, Zhenda Lu, Yi Cui,* and Zhenan Bao*

High-performance lithium-ion batteries are of high demand for portable electronic devices, electric vehicles, and renewable energy storage. Over the years, great effort has been devoted toward developing high capacity electrode materials to boost the energy density.[1–3] Si holds great promise for next-generation anodes because they can deliver more than 10× theoretical capacity ($\approx$4200 mAh g^{-1}) over conventional graphite-based materials ($\approx$370 mAh g^{-1}). The major problem faced by Si anodes is their large volume change (>300%) during repeated lithiation and delithiation processes.[4–7] This results in degradation of structural integrity and rapid decay of electrode capacity due to loss of electrical contact and progressive growth of a solid-electrolyte-interphase (SEI) on the Si surface.[8–12] To address the stability issue, various Si nanostructures including nanoparticles,[11,13–15] nanowires,[6] core–shell nanowires,[16–18] nanotubes,[10,19,20] yolk–shell nanoparticles,[21,22] pomegranate structures,[12] nanoporous structures,[23–27] and nanocomposites[28–35] have been developed to improve cycle stability. It has been shown that Si needs to be <150 nm in diameter for particles and <250 nm in diameter for nanowires to avoid mechanical fracture.[36–38] However, these critical sizes are below ($\approx$500 nm in diameter) and can be produced by existing low cost and scalable mechanical milling processes. Therefore, it is desirable to develop materials methodology to effectively utilize low-cost large particles, while still achieving excellent battery cycling performance. However, past attempts in using large Si particles had showed fast capacity decay.[4,25,39–41]

The second challenge for new battery development is the significant decay in specific capacity upon high mass loading, resulting in low areal capacity. For practical applications, high areal capacity is crucial for high gravimetric or volumetric energy density based on the whole cell. Currently, only a few reported Si nanostructures can reach an areal capacity of >3 mAh cm^{-2}.[12,27]

Recently, we reported the use of self-healing polymers (SHPs) to stabilize low-cost Si microparticle (SiMP) anodes. SHPs have both mechanical and electrical healing capabilities, which allow cracks and damages to the conduction paths to repeatedly heal during battery cycling. SiMP electrodes with 90 cycles and capacity loading of $\approx$1 mAh cm^{-2} and 45 cycles with areal capacity loading of 1.9 mAh cm^{-2} were reported.[42] However, long-term cycling stability and high Si mass loading have not yet been achieved. Similarly, a binder incorporating Meldrum's acid showed some self-healing effect that can improve the cycling performance of Si electrodes. Yet such electrodes were still based on costly Si nanoparticles (<100 nm) and low mass loading.[43]

Here, we demonstrate high areal capacity (3–4 mAh cm^{-2}) and stable cycling for more than 140 cycles using low-cost large Si particles. This major advancement is enabled by: 1) Our new electrode design with 3D spatial distribution of SHP into Si electrodes to promote more effective self-healing. 2) Our ability to control the Si particle sizes to maintain high cycling stability and low cost.

Generally, stable electrode function relies on the integrity of both the ionic and electronic conductive pathways and a stable electrode–electrolyte interface. Conventional Si electrodes are fabricated using a polymer binder (e.g., polyvinylidene difluoride (PVdF), carboxymethyl cellulose (CMC), alginate, conducting polymers) to hold Si particles with conductive agents (e.g., carbon black (CB)).[4,15,25,44,45] Due to the low stretchability (<10%) and weak interaction with Si particles, upon electrode cycling, a large stress generated by the huge volume change will break both the Si particles and the rigid conductive composite binders. Additionally, the exposed surfaces consume electrolyte and rapidly reduce electrode capacity. Our SHP (Figure S1, Supporting Information)[42] contains abundant hydrogen bonds binding sites with Si particle surfaces, thus providing good adhesion between the SHP and Si particles. Combining with CB, the SHP composites (SHP/CB) have good electrical conductivity ($\approx$0.25 S cm^{-1}). Moreover, the SHP is highly stretchable (up to $\approx$300% strain without breaking) and capable of viscous flow.[42] Even after rupture, the conductive pathway and binding with Si particles can recover and the cracks can self-heal. As a result, electrode function can be maintained, leading to improved cycling performance.

The cycling performance of the self-healing Si electrodes depends on the healing capability of the polymer binder.

Dr. Z. Chen, Dr. C. Wang, J. Lopez, Prof. Z. Bao
Department of Chemical Engineering
Stanford University
Stanford, CA 94305, USA
E-mail: zbao@stanford.edu
Dr. Z. Lu, Prof. Y. Cui
Department of Materials Science and Engineering
Stanford University
Stanford, CA 94305, USA
E-mail: yicui@stanford.edu
Prof. Y. Cui
Stanford Institute for Materials and Energy Sciences
SLAC National Accelerator Laboratory
Menlo Park, CA 94205, USA

ADVANCED
ENERGY
MATERIALS
www.advenergymat.de

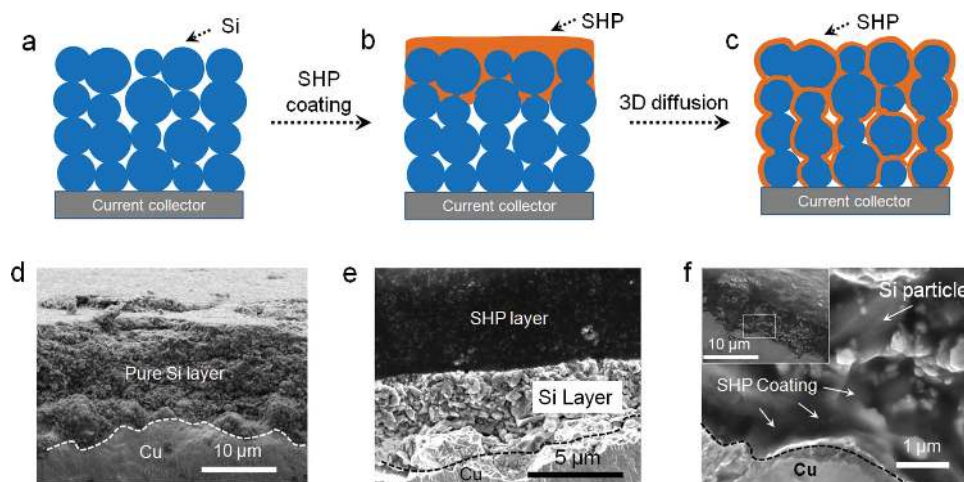www.MaterialsViews.com

COMMUNICATION

Figure 1. Electrode design toward tuning spatial distribution of SHP/CB in Si layer. a–c) Schematic design of Si-SHP/CB electrodes. d–f) SEM images of Si and Si-SHP/CB electrodes. d) Pure Si electrodes made from Si particles. e) SHP/CB layer coated on top of Si electrodes with one-time blading. f) Si electrodes filled with SHP/CB forming a 3D distribution inside electrodes from repeated blading under heating.

Accordingly, it is essential to build a robust interface between Si particles and the SHP to maintain electrode integrity. At the electrode level, the electrical connection between particles can be damaged by the large volume change of Si lithiation/delithiation, resulting in capacity decay. At the individual particle level, crack formation can cause the loss of electrical contact and detachment of active materials. In our previous study, we coated SHP only on top of the Si particle electrodes, at a thickness of 200 nm–3 μm.[42] Therefore, a significant fraction of Si material was not in close proximity to the SHP. In our new electrode design described herein, we have intentionally distributed the SHP 3D into the Si particle layer, in order to provide a faster healing response owing to the shorter diffusion lengths of SHP to the generated fracture sites.

Figure 1a–c shows the schematic of the 3D design compared with top layer coating. Si electrodes were fabricated by coating a Si particle slurry on Cu substrates, followed by drying and calendaring (Figure 1a). SHP/CB polymer composite was then coated on the Si electrode using a blade to form the top layer (Figure 1b). Repeatedly blading under heating condition (120≈150 °C), is crucial to allow the SHP/CB to infiltrate into the entire thickness of the Si layer, forming a 3D distribution of SHP/CB inside the Si electrode (Si-SHP/CB, Figure 1c). The bulk density of Si film was calculated to be 1.0–1.1 g cm^{-3} for particles with ≈800-nm diameter, corresponding to a porosity of ≈60% (Figure 1d). After coating the SHP/CB on the top layer of Si film, without heating, a clear boundary between Si and Si-SHP/CB can be observed from the cross-section view of the electrodes (Figure 1e). After repeated coating under heating, a 3D spatial distribution of SHP/CB can be clearly seen inside the whole Si electrode (Figure 1f).

Since the healing of fractures relies on interactions between SHP and Si particles, we hypothesize that particle sizes may influence the healing behavior. For large SiMPs (e.g., a few microns), a full lithiation/delithiation not only produces large cracks, but also induces pulverization with a large number of small cracks between fragments. To maintain electrode activity, conductive pathways need to be rebuilt through

diffusion of SHP into these cracks. This requires a continuous healing pathway, and is especially difficult. As a result, capacity loss occurs due to increased dead zones where electron and ion transport are interrupted. In contrast, smaller Si particles have higher surface areas and more binding sites with SHP. They are also subjected to less pulverization. Even if fractures were to occur, the diffusion of SHP and healing of small cracks can proceed more efficiently due to a shorter diffusion length. In the extreme case of ultrasmall SiNPs (e.g., <150 nm), they do not present particle fracture[36,37,46] and can be fully protected by the stretchable SHP layer (>300% stretchability).

To verify the above hypothesis, Si-SHP/CB electrodes were fabricated using Si particles with different sizes that range in between 250 nm and 3.5 μm (see "Experimental Section"). They were obtained by a simple yet effective solution precipitation–floatation selection process (Figure S2, Supporting Information). As shown in **Figure 2**, different electrodes showed quite different cycling performances. For 3.5 μm SiMPs (Figure 2a), most of the Si electrode consists of large particles and the electrodes showed a low-initial delithiation capacity (≈1100 mAh g^{-1} at C/20), which may be due to slow lithium-ion diffusion and high lithiation overpotential caused by activation energy barrier of large particles.[4,5,47] The rapid capacity decrease upon cycling is attributed to the insufficient healing capability of the SHP binder for very large Si particles as discussed above. 1-μm SiMP electrodes (Figure S3, Supporting Information) showed a much higher initial delithiation capacity of 2510 mAh g^{-1}. In this case, although more than 50% of particles are ≈1 μm (Figure S3b, Supporting Information), a small number of larger particles (2–6 μm) contributed to >80% of the total volume (Figure S3c, Supporting Information). Although gradual capacity decay was still observed, the capacity retention was clearly improved, as ≈70% of capacity was retained even after about 100 cycles (Figure S3d, Supporting Information). The increased cycling stability was ascribed to the enhanced healing capability from a better Si-SHP interface. As the particle size is reduced to around 800 nm (Figure 2b), the electrodes are able to deliver
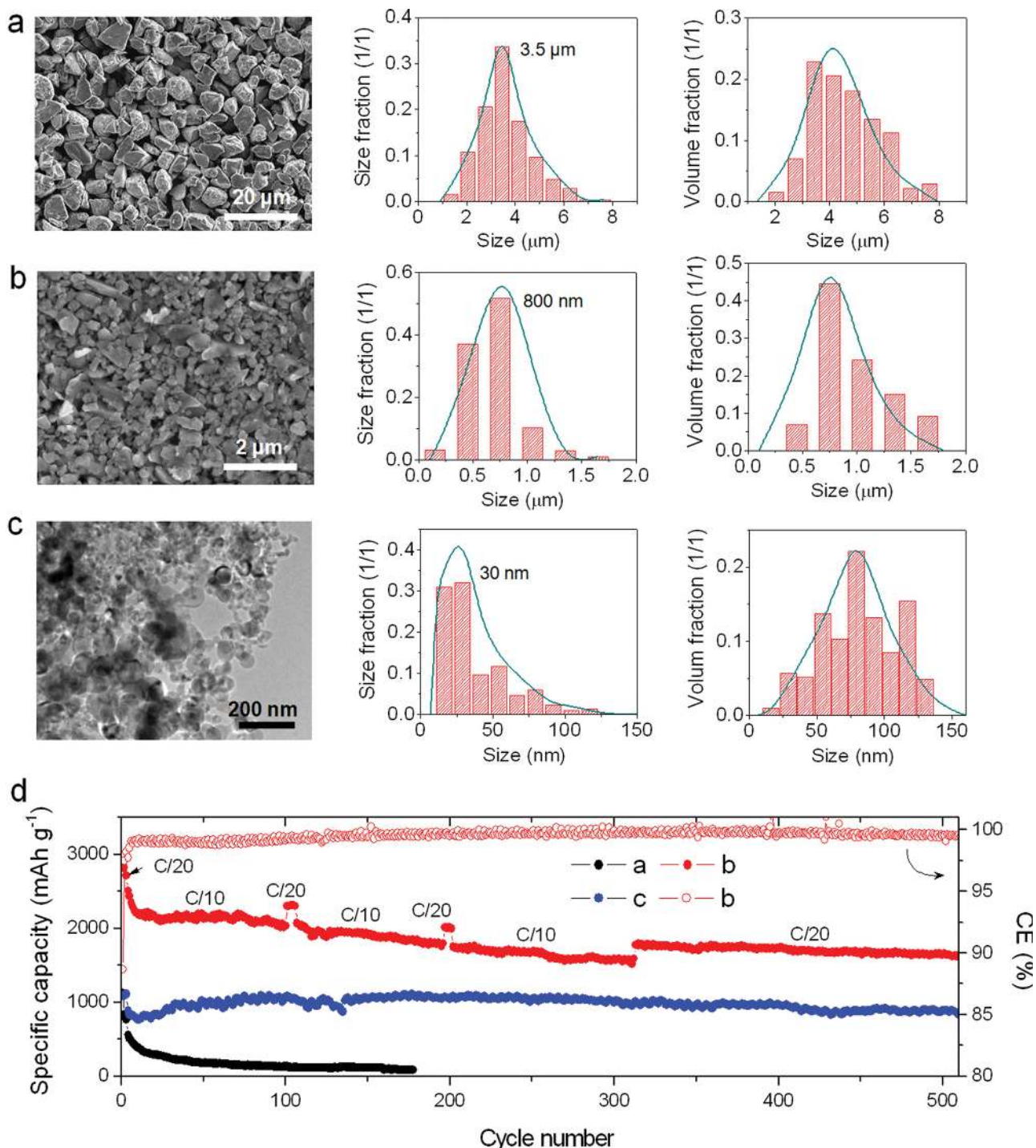
www.MaterialsViews.com

ADVANCED
ENERGY
MATERIALS
www.advenergymat.de

COMMUNICATION

Figure 2. Effect of Si particle size on electrode cycling performance. a–c) SEM images (left) of Si particles, corresponding particle size distributions (middle) and volume fraction of each particle size (right) obtained from the precipitation–floatation-based selection process. d) Cycling stability of different Si-SHP/CB electrodes (a, b, and c correspond to Si particles shown above) with Si mass loading of 0.5–0.6 mg cm^{-2}.

an even higher initial delithiation capacity of 2620 mAh g^{-1} (corresponding to an areal capacity of 1.3 mAh cm^{-2}) due to the faster lithium reaction kinetics. While ≈95% of whole Si volume is from particles with diameter of 800 nm or larger, the electrodes maintained an impressive ≈80% of their initial capacity after 500 cycles. This comparative study confirms that carefully

reduced Si particle size contributes to enhanced Si-SHP interface and better electrode structure.

As expected, further decreasing the Si particle size provides an even better cycling stability. For 500- and 250-nm Si particles (Figures S4 and S5, Supporting Information), their initial delithiation capacity was ≈2600 and 2200 mAh g^{-1}, and the electrode capacity

retention was ≈80% after 550 and 600 cycles, respectively. Even though the particle size decreased dramatically, the first-cycle CE remained similar (86%–88%) (Figure S6, Supporting Information), which are much higher than common nanostructured or nanoporous Si electrodes.[11,12,15,27,48] For 30-nm SiNPs (Figure 2c), the electrodes showed no obvious capacity decay even after 1000 cycles (Figure S7, Supporting Information), regardless of the relatively low first-cycle CE (73%). Note that the relatively low capacity of SiNPs-based electrodes may be due to their large electrode series resistance (ESR) (Figures S7 and S8, Supporting Information) resulted from the oxide layer on the SiNPs surface and relatively small pore size in the electrodes. Such a stable cycling performance is comparable to the most effective nanostructured Si electrodes while our electrode here has a higher mass loading. Clearly, this study indicates that optimal particle size distribution in Si-SHP/CB electrodes is essential for good electrode performance. To avoid low CE and volumetric capacity, large particle size will be needed. In addition, to achieve high specific capacity and stable cycling performance, a relative small size is preferred. The net result obtained from this study suggests that Si particles with 800-nm peak size and a small size distribution (500 nm–1.5 μm) can meet the requirement for both high CE, stable cycling performance, and low cost.

High areal mass loading is a critical requirement for high-performance practical batteries to reduce the weight and size of the whole cell.[49] However, many previous works only reported improved cycling life of Si electrodes based on low-Si mass loadings.[10,11,15,19] Making thicker Si electrodes introduces fundamental challenges that do not occur in thinner ones, including high ESR, large particle–electrolyte, interface and increased electrode-level disintegration. For these reasons, high-areal-capacities (>2 mAh cm^{-2}) have rarely been reported. Our above study suggests that 800-nm Si particles enable stable cycling performance and can be readily separated from very low-cost commercial Si powder. This size range is also easily accessible by the well-established ball-milling technique (e.g., jet milling).[50] Using our generated Si particles, we fabricated Si-SHP/CB electrodes with high Si mass loading (1–1.6 mg cm^{-2}), and we proceed to successfully demonstrate stable cycling at high areal capacity (3–4 mAh cm^{-2}).

To be specific, CB (5 wt%) was added to prevent large ohmic resistance in the Si layer for thick electrodes (Figure S9, Supporting Information). As Si mass loading increased from 0.22 to 1.6 mg cm^{-2}, the electrode areal capacity can be almost linearly enhanced from 0.6 to 4.1 mAh cm^{-2} (**Figure 3**a and Supporting Information, Figure S10), suggesting that high
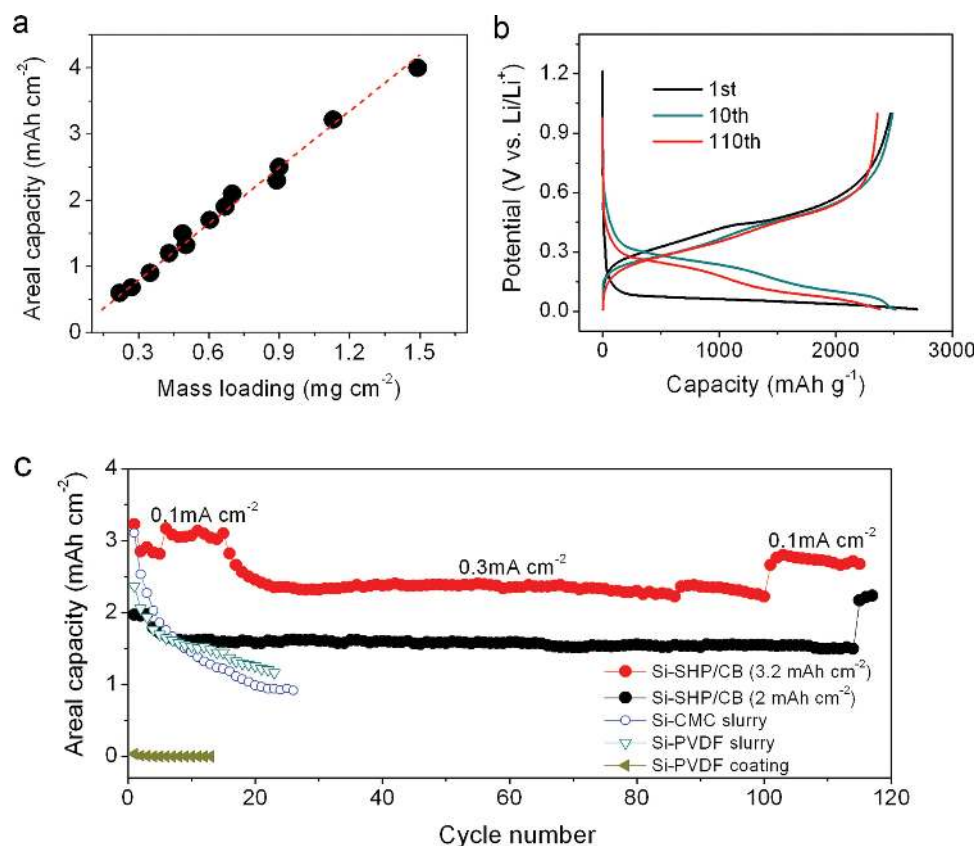

Figure 3. Performance of thick Si-SHP/CB electrodes. a) Dependence of electrode areal capacity (first cycle delithiation capacity) on the Si mass loading of Si-SHP/CB electrodes. b) Galvanostatic charge/discharge curves (at 0.1 mA cm^{-2}) of a thick Si-SHP/CB electrode at different cycles. c) Comparison of cycling stability of thick Si electrode fabricated using different methods (Si-SHP/CB: 3D SHP/CB coated electrodes; Si-CMC slurry: Si electrodes made by slurry coating with CMC as binder; Si-PVDF slurry: Si electrodes made by slurry coating with PVDF as binder; Si-PVDF coating: Si electrodes made by coating PVDF layer on Si film. The Si mass loading of each CMC- or PVDF-based electrode was ≈1.0 mg$_{Si}$ cm^{-2}). The 3.2 mAh cm^{-2} Si-SHP/CB electrode was cycled at 0.1 mA cm^{-2} for first 5 and last 15 cycles. The 2 mAh cm^{-2} Si-SHP/CB electrode was cycled at 0.1 mA cm^{-2} for first and last 3 cycles and at 0.3 mA cm^{-2} for the rest cycles.

electrochemical activity was preserved in our high mass loading electrodes. All the Si-SHP/CB electrodes maintained typical features of Si as shown by their representative cyclic voltam-mogram (Figure S11, Supporting Information) and galvano-static charge/discharge curves (Figure 3b). More importantly, these electrodes still maintained excellent cycling stability. For example, a Si-SHP/CB electrode with high mass loading of 1.13 mg$_{si}$ cm^{-2} (0.6 mg of SHP/CB) delivered an initial areal capacity of ≈3.22 mAh cm^{-2} at a current of 0.1 mA cm^{-2} (cor-responding to Si specific capacity of 2850 mAh g$_{si}$$^{-1}$). Based on electrode thickness and mass loading, the volumetric capacity of the thick Si-SHP/CB electrode reached ≈3135 and 1540 mAh cm^{-3} (before and after volume expansion, see Experi-mental Section), which is (i) more than twice as compared to graphite anodes; and (ii) significantly higher than most of pre-vious nanostructured Si electrodes (600–1500 mAh cm^{-3} before volume expansion).[11,12,51,52] The capacity slightly decreased to ≈2.95 mAh cm^{-2} (2610 mAh g$_{si}$$^{-1}$) after three activation cycles and fully recovered after 5 cycles at the same rate. The decrease in capacity after initial cycle may be due to the frac-ture of particles and cracks of electrodes. The following capacity recovering behavior is a strong indication of the occurrence of self-healing processes in the conduction pathways. The capacity remained stable in the following cycles at a current of 0.3 mA cm^{-2}, and a high areal capacity of 2.72 mAh cm^{-2} was retained after ≈120 cycles, corresponding to capacity retention of 85%. Continuous cycling on the electrode to 130 cycles led to a stable charge capacity; however, the cell started to fail due to the lithium counter electrode as a result of lithium dendrite formation (a common occurrence in high mass loading cells, Figure S12, Supporting Information). With a slightly lower mass loading (0.72 mg$_{si}$ cm^{-2}), Si-SHP/CB electrode showed an initial capacity of 1.97 mAh cm^{-2} (2736 mAh g$_{si}$$^{-1}$) at a current of 0.1 mA cm^{-2} and can be cycled very stably over 100 cycles

at 0.3 mA cm^{-2} (Figure 3c). After returning to low current, the total capacity slightly increased to 2.2 mAh cm^{-2}, which may be again due to electrochemical activation and self-healing effect. Continuous cycling showed that ≈90% of initial capacity can be retained after 240 cycles (Figure S13, Supporting Information). For an even higher mass loading (1.6 mg$_{si}$ cm^{-2}), the revers-ible areal-capacity reached ≈ 4.2 mAh cm^{-2}, and the electrode can be stably cycled to over 140 cycles (Figure S14, Supporting Information). In comparison, Si electrodes with the same Si particles and similar mass loadings (≈1 mg cm^{-2}) made from slurry-coating method using CMC or PVDF as binder showed rapid capacity decay after a few cycles; thick Si electrodes coated with PVDF film (0.6 mg cm^{-2}) showed negligible capacity, which was due to the slow Li$^+$ transport in the thick PVDF film as confirmed by electrochemical impedance spectroscopic (EIS) test (Figure S15, Supporting Information).

The excellent cycling stability observed for the high mass loading Si-SHP/CB electrodes is attributed to its robust struc-ture, conferred by the 3D coating of SHP/CB. Both **Figure 4**a and Figure S16 (Supporting Information) show the surface morphologies of the thick electrodes at different magnifications; the relatively rough surfaces are due to the adhesion of SHP/CB to the large Si particles. Figure 4b shows the SEM image of the typical surface morphology of a thick Si-SHP/CB electrode after 100 cycles. In comparison with a fresh electrode (Figure 4a), the electrode surface became even more rough after cycling, which could be due to the repeated volume change of the whole electrode followed by the stretching and shrinkage of SHP/CB. Nevertheless, no obvious cracks can be observed from the sur-face, as well as from the cross-section SEM images (Figure 4c). Moreover, a relatively dense structure without distinguishable Si particles (Figure S17, Supporting Information) was observed from its cross-section image, indicating that most of the active materials were involved in the electrode reactions and remained
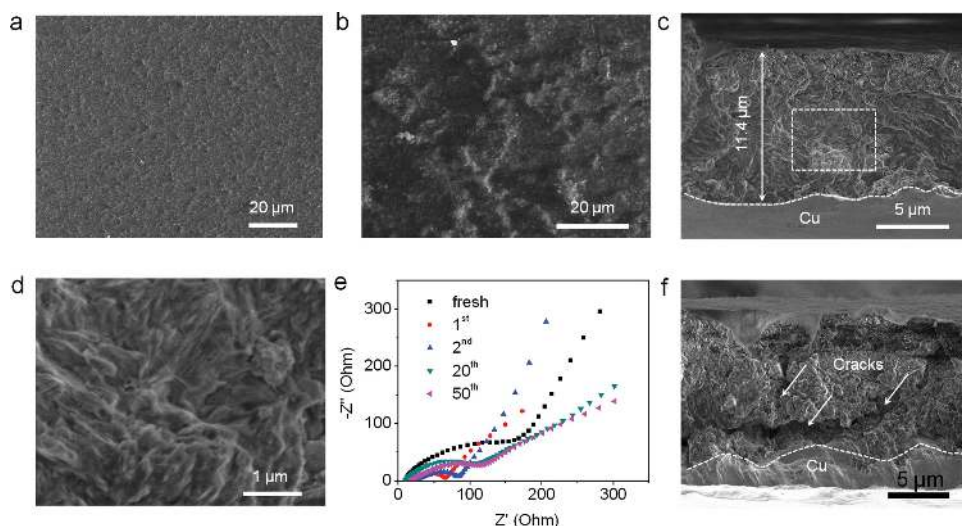

Figure 4. Structure and cell impedance of high mass loading Si-SHP/CB electrodes before and after cycling. Representative SEM image of thick 3D Si-SHP/CB electrode before a) and after b) cycling. c,d) Cross-section SEM images of thick 3D Si-SHP/CB electrode after cycling, the selected area in (c) is shown in (d), no obvious cracks were observed in the electrode. e) Nyquist plots of the high mass loading 3D Si-SHP/CB electrodes at dif-ferent cycling status. A transition between activation and stabilization of electrode ESR can be observed with electrode cycling. The electrode ESR first decreased due to activation of Si, and then increased and stabilized due to continuous particle fraction and self-healing of cracks. f) Cross-section SEM image of surface SHP/CB-coated high mass loading Si electrode showing large cracks after cycling.

in intimate electrochemical contact (Figure 4d). In addition, we observed that even electrode thickness increased by ≈2.1× after full lithiation; the thickness of delithiated electrode after repeated cycling increased by only ≈20% compared with fresh electrodes, (Figure 1f) which suggests that the 3D-SHP network in Si layer can provide strong tolerance to buffer electrode volume change and particle rupture. EIS measurement further confirms the robust electrode structure enabled by the SHP (Figure 4e). The ESR dramatically decreased after the first cycle, which suggests an activation process. This can be attributed to size reduction of Si particles after fracture and the lithiation of Si particles. The ESR increased slightly in the following cycles, which is possibly due to the diffusion of SHP/CB or growth of SEI on Si surface. Nevertheless, the ESR was stabilized after 20 cycles, showing that good electrode conductivity and ion diffusion was maintained stably by SHP/CB.

To further confirm that the 3D distribution of SHP in electrodes is essential, thick Si-SHP/CB electrodes were also tested by only applying a surface coating layer (Figure 1e). While thin (3 μm) Si electrodes showed better cycling stability (90 cycles),[42] thicker electrodes with initial areal capacity of ≈2.1 mAh cm^{-2} subject to the same cycling showed capacity loss of 20% after 60 cycles (Figure S18, Supporting Information). Even with an extra healing step performed by resting the cycled cell, the electrode capacity could not be recovered, which may be due to the following two reasons: i) Thick SEI formed on the surface of unprotected Si particles before SHP/CB start to heal, which gradually blocked charge transfer. ii) Large cracks cannot be effectively repaired during cycling, since the diffusion of SHP to the generated cracks is more difficult. Figure 4f clearly shows a typical cross-section SEM image of surface-coated high mass loading Si-SHP/CB electrode after cycling. The large cracks indicate that electrode was not robust enough to maintain its inner structural integrity and electrochemical function. Even worse, pure Si thick electrodes without any SHP/CB coating showed more rapid capacity decay, and the capacity kept decreasing even when a similar resting step was reapplied (Figure S19, Supporting Information).

So far, few high-areal-capacity Si electrodes have been achieved and they all used more sophisticated nanostructure designs. For example, a micron-sized Si–C composite with Si nanocrystals can be synthesized from expensive SiO microparticles followed by a high temperature carbon coating to give an areal capacity of ≈1.8 mAh cm^{-2} over 200 cycles.[24] A pomegranate-like hierarchical structured electrode from SiNP can be made through a multistep synthesis to boost areal capacity to ≈3.7 mAh cm^{-2} with a cycling life of 100×.[12] Specially designed binder also enabled SiNP-based electrodes with a capacity of ≈4 mAh cm^{-2} and ≈50× cycle life.[53,54] The mesoporous Si sponge with very high porosity (≈80%) showed an areal capacity of ≈1.5 mAh cm^{-2} with ≈92% of capacity retention over 300 cycles, and areal capacity of 3–4 mAh cm^{-2} have been also demonstrated for tens of cycles.[27] Our high mass-loading Si-SHP/CB electrodes showed comparable, or even longer, cycling life than the above described high-performance electrodes but with very low-cost materials and fabrication process. It should be mentioned that Si nanostructures often possess high surface areas, large interparticle resistance and low-tap density. In addition, carbon coating often results in irreversible lithium uptake

into amorphous carbon textures.[12,31,46] These features usually render low CE and low volumetric capacity, making it problematic for full cell fabrication.

In summary, we have demonstrated an effective electrode design approach toward low-cost Si electrodes with long cycling life and high mass loading. The 3D distribution of SHP together with optimal Si particle size resulted in electrodes with significantly improved robustness and a high degree of electrode stability even after long cycling. Our electrode approach possesses key advantageous features: i) very high areal capacity that is close to practical battery requirement; ii) our materials are based on low-cost metallurgical Si powders; and iii) optimal performance can be achieved by selecting appropriate Si particle size using scalable precipitation–floatation process or ball milling.

We note that there are several remaining challenges to be addressed. First, the continuous growing of SEI layer can lead to electrolyte consumption and nonideal CE (99.5% for stable cycling). Our previous work showed that the surface of conducting SHP/CB had negligible SEI formation;[42] thus, the surface of the newly exposed Si after cracking is likely the major contributor to SEI formation. In this context, a SHP with fast flow and bonding will be needed to instantaneously protect the Si surface to avoid SEI growth. Second, the electrical healing of our electrodes was based on CB distributed in SHP to provide electrical conductivity. Upon repeatedly stretching (Si expanding) and relaxation (Si shrinking), the CB particles may slowly form aggregates in the polymer matrix. As a result, the conductivity will decrease and capacity will be lost. Therefore, more interaction between the CB particles and SHP may improve the stability. Last, the thick Si-SHP/CB electrodes had moderate rate capability mainly due to the relatively slow reaction kinetics. Low-cost approaches for engineering electrode porosity and utilizing Si particles with conductive coatings (e.g., graphitized carbon and metal) may improve both the interface stability and electrode kinetics. Together with future development of an intrinsically conductivity SHP, Si electrodes with even longer electrode cycling life and higher mass loading can be realized.

Experimental Section

Synthesis of SHP/CB: Self-healing polymer and SHP/CB composite were prepared using the method described earlier.[42]

Size-Selected Si Particles: A precipitation–floatation process was used to separate Si particles. To obtain Si particles with different sizes, commercial metallurgical-grade Si powders (ABRC Inc., 0.4 g, 99.995% purity) with a broad range of size (250 nm–8 μm) were dispersed in ethanol (10 mL) by ultrasonication. After 10 min, the suspension was settled down and particles with different sizes precipitated or floated at different time scales. For example, large particles precipitated from the suspension fast while small particles floated in the suspension for longer time. By taking the uplevel suspension or sediment with different floatation time (e.g., 10, 20, 30, 60, and 120 min), Si particles with different sizes were obtained. For example, Si particles with size distributed from 500 nm to 1.5 μm and peak size of 800 nm was obtained by filtrating the suspension with floatation time between 20 and 30 min. Such particles accounts for 15–20 wt% of the total commercial Si powders. By repeating the precipitation–floatation process for selected samples, Si particles with further narrowed-size distribution can be obtained. The particles with 250-nm diameter account for <1% of the total weight.

Ultrasmall SiNPs made from plasma-enhanced chemical vapor deposition process was also used. In the main text, for simplicity reason, all

the separated Si particles are identified by their peak size regardless of their size distributions. For example, particles with size distributed from 500 nm to 1.5 µm and peak size at 800 nm are defined as 800-nm particles. The Si particle size distribution was obtained by counting 300 particles from SEM or TEM images. Then a corresponding volume fraction of each size was calculated based on size distribution by assuming a regular shape.

Electrochemical Characterization: To make electrodes with moderate mass loading, 0.1 g of Si size-selected Si particles or SiNPs (MTI cooperation) was dispersed in 4 mL of ethanol by sonication. To make thick electrodes (i.e., >1 mg$_{si}$ cm^{-2}), Si (95 mg), and CB (5 mg) were mixed and homogenized in ethanol. Working electrodes were prepared by drop-casting the Si (or Si–CB) suspension onto 10 µm Cu discs (Fukuda) with an area of ≈1 cm^2. After drying at room temperature followed by calendaring, uniform electrodes were prepared with a controlled Si mass loadings. The Si electrodes were heated to 120–150 °C on a hot plate. The SHP/CB composite was then melted and coated on Si electrodes with a sharp blade to form the top layer; repeated blading under heating removed the excessive surface SHP/CB and facilitated its migration to form 3D coating in Si electrodes. The weight ratio between Si active materials and polymer composite was about 2:1.

To examine the effect of Si particle size on the electrochemical performance of 3D Si-SHP/CB electrodes, coin cells were fabricated by sandwiching working electrode, separator (Celgard 2400) and lithium disc (≈1 cm^2) counter electrodes. The mass loading of Si particles in each electrode was controlled at 0.5–0.6 mg$_{si}$ cm^{-2} to minimize the possible kinetic issues in thick electrodes, including large ohmic resistance, ion diffusion resistance, etc. All the electrodes were cycled at a rate of C/20 (C/n = charge/discharge in n h) in the first 3 cycles for activation and at C/10 in the following cycles. For some of the separated Si particles electrodes, interval cycles at slower or higher rates were introduced during cycling to monitor the full capacity or rate performance. For thick electrodes (>1 mg$_{si}$ cm^{-2}), relatively lower rates were used in initial cycles for activation (e.g., C/30). The electrolyte for all tests was 1 M LiPF$_6$ in ethylene carbonate/diethylcarbonate/vinyl carbonate/fluoroethylenecarbonate (1:1:0.005:0.05 v/v/v/v), and separators (25 µm) from Asahi Kasei Co. were used. Cyclic voltammetry and EIS measurement were performed by VMP3 (Bio-Logic) for, and BT 2000 (Arbin Instrument) for galvanostatic charge/discharge cycling. The cycling rates were calculated by assuming theoretical capacity of 4200 mAh g^{-1} for Si. The CE was calculated as (C$_{discharge}$/C$_{charge}$) × 100%, where C$_{charge}$ and C$_{discharge}$ were the capacity of the anodes for lithiation and delithiation. All areal capacity was based on Si delithiation capacity. The electrode volumetric capacity before volume expansion was calculated based on a measured density of 1.1 g cm^{-3}. By assuming a volume expansion ratio of 3 at full lithiation capacity of 4200 mA g^{-1}, the volume change ratio R at a lithiation capacity of C$_{charge}$ was estimated by R = C$_{charge}$/4200 mAh g^{-1} × 3. Then the density d$_{charge}$ of lithiated electrode can be estimated by d$_{charge}$ = 1.1/R. The volumetric capacity after expansion was calculated based on such density.

[1] J. M. Tarascon, M. Armand, *Nature* **2001**, *414*, 359.
[2] M. Armand, J. M. Tarascon, *Nature* **2008**, *451*, 652.
[3] B. Dunn, H. Kamath, J. M. Tarascon, *Science* **2011**, *334*, 928.
[4] M. N. Obrovac, L. Christensen, *Electrochem. Solid-State Lett.* **2004**, *7*, A93.
[5] M. N. Obrovac, L. J. Krause, *J. Electrochem. Soc.* **2007**, *154*, A103.
[6] C. K. Chan, H. Peng, G. Liu, K. McIlwrath, X. F. Zhang, R. A. Huggins, Y. Cui, *Nat. Nanotechnol.* **2008**, *3*, 31.
[7] X. H. Liu, J. W. Wang, S. Huang, F. Fan, X. Huang, Y. Liu, S. Krylyuk, J. Yoo, S. A. Dayeh, A. V. Davydov, S. X. Mao, S. T. Picraux, S. Zhang, J. Li, T. Zhu, J. Y. Huang, *Nat. Nanotechnol.* **2012**, *7*, 749.
[8] C.-M. Park, J.-H. Kim, H. Kim, H.-J. Sohn, *Chem. Soc. Rev.* **2010**, *39*, 3115.
[9] H. Wu, Y. Cui, *Nano Today* **2012**, *7*, 414.
[10] H. Wu, G. Chan, J. W. Choi, I. Ryu, Y. Yao, M. T. McDowell, S. W. Lee, A. Jackson, Y. Yang, L. Hu, Y. Cui, *Nat. Nanotechnol.* **2012**, *7*, 310.
[11] H. Wu, G. Yu, L. Pan, N. Liu, M. T. McDowell, Z. Bao, Y. Cui, *Nat. Commun.* **2013**, *4*, 1943.
[12] N. Liu, Z. Lu, J. Zhao, M. T. McDowell, H.-W. Lee, W. Zhao, Y. Cui, *Nat. Nanotechnol.* **2014**, *9*, 187.
[13] M.-H. Ryou, J. Kim, I. Lee, S. Kim, Y. K. Jeong, S. Hong, J. H. Ryu, T.-S. Kim, J.-K. Park, H. Lee, J. W. Choi, *Adv. Mater.* **2013**, *25*, 1571.
[14] Y. K. Jeong, T.-W. Kwon, I. Lee, T.-S. Kim, A. Coskun, J. W. Choi, *Nano Lett.* **2014**, *14*, 864.
[15] G. Liu, S. Xun, N. Vukmirovic, X. Song, P. Olalde-Velasco, H. Zheng, V. S. Battaglia, L. Wang, W. Yang, *Adv. Mater.* **2011**, *23*, 4679.
[16] L. Hu, H. Wu, Y. Gao, A. Cao, H. Li, J. McDough, X. Xie, M. Zhou, Y. Cui, *Adv. Energy Mater.* **2011**, *1*, 523.
[17] T. D. Bogart, D. Oka, X. Lu, M. Gu, C. Wang, B. A. Korgel, *ACS Nano.* **2013**, *8*, 915.
[18] T. H. Hwang, Y. M. Lee, B.-S. Kong, J.-S. Seo, J. W. Choi, *Nano Lett.* **2012**, *12*, 802.
[19] B. Wang, X. Li, X. Zhang, B. Luo, Y. Zhang, L. Zhi, *Adv. Mater.* **2013**, *25*, 3560.
[20] M.-H. Park, M. G. Kim, J. Joo, K. Kim, J. Kim, S. Ahn, Y. Cui, J. Cho, *Nano Lett.* **2009**, *9*, 3844.
[21] N. Liu, H. Wu, M. T. McDowell, Y. Yao, C. Wang, Y. Cui, *Nano Lett.* **2012**, *12*, 3315.
[22] S. Chen, M. Gordin, R. Yi, G. Howlett, H. Sohn, D. Wang, *Phys. Chem. Chem. Phys.* **2012**, *14*, 12741.
[23] H. Kim, B. Han, J. Choo, J. Cho, *Angew. Chem Int. Ed.* **2008**, *47*, 10151.
[24] R. Yi, F. Dai, M. L. Gordin, S. Chen, D. Wang, *Adv. Energy Mater.* **2013**, *3*, 295.
[25] B. M. Bang, H. Kim, H.-K. Song, J. Cho, S. Park, *Energy Environ. Sci.* **2011**, *4*, 5013.
[26] J. Cho, *J. Mater. Chem.* **2010**, *20*, 4009.
[27] X. Li, M. Gu, S. Y. Hu, R. Kennard, P. Yan, X. Chen, C. Wang, M. J. Sailor, J.-G. Zhang, J. Liu, *Nat. Commun.* **2014**, *5*, 4105.
[28] J.-K. Lee, M. C. Kung, L. Trahey, M. N. Missaghi, H. H. Kung, *Chem. Mater.* **2008**, *21*, 6.
[29] A. Magasinski, P. Dixon, B. Hertzberg, A. Kvit, J. Ayala, G. Yushin, *Nat. Mater.* **2010**, *9*, 353.
[30] J. Ji, H. Ji, L. L. Zhang, X. Zhao, X. Bai, X. Fan, F. Zhang, R. S. Ruoff, *Adv. Mater.* **2013**, *25*, 4673.
[31] Y. S. Hu, R. Demir-Cakan, M.-M. Titirici, J.-O. Müller, R. Schlögl, M. Antonietti, J. Maier, *Angew. Chem Int. Ed.* **2008**, *47*, 1645.
[32] X. Zhou, L.-J. Wan, Y.-G. Guo, *Small* **2013**, *9*, 2684.
[33] X. Zhou, A.-M. Cao, L.-J. Wan, Y.-G. Guo, *Nano Res.* **2012**, *5*, 845.
[34] B. Liu, P. Soares, C. Checkles, Y. Zhao, G. Yu, *Nano Lett.* **2013**, *13*, 3414.
[35] D. S. Jung, T. H. Hwang, S. B. Park, J. W. Choi, *Nano Lett.* **2013**, *13*, 2092.

COMMUNICATION

[36] X. H. Liu, L. Zhong, S. Huang, S. X. Mao, T. Zhu, J. Y. Huang, *ACS Nano* **2012**, *6*, 1522.

[37] M. T McDowell, I. Ryu, S. W. Lee, C. Wang, W. D. Nix, Y. Cui, *Adv. Mater.* **2012**, *24*, 6034.

[38] S. W. Lee, M. T. McDowell, L. A. Berla, W. D. Nix, Y. Cui, *Proc. Natl. Acad. Sci. USA* **2012**, *109*, 4080.

[39] M. Wu, J. E. C. Sabish, X. Song, A. M. Minor, V. S. Battaglia, G. Liu, *Nano Lett.* **2013**, *13*, 5397.

[40] U. Kasavajjula, C. Wang, A. J. Appleby, *J. Power Sources* **2007**, *163*, 1003.

[41] J. Guo, X. Chen, C. Wang, *J. Mater. Chem.* **2010**, *20*, 5035.

[42] C. Wang, H. Wu, Z. Chen, M. T. McDowell, Y. Cui, Z. Bao, *Nat. Chem.* **2013**, *5*, 1042.

[43] T. W. Kwon, Y. K. Jeong, I. Lee, T.-S. Kim, J. W. Choi, A. Coskun, *Adv. Mater.* **2014**, *26*, 7979.

[44] J.-S. Bridel, T. Azaïs, M. Morcrette, J.-M. Tarascon, D. Larcher, *J. Electrochem. Soc.* **2011**, *158*, A750.

[45] I. Kovalenko, B. Zdyrko, A. Magasinski, B. Hertzberg, Z. Milicev, R. Burtovyy, I. Luzinov, G. Yushin, *Science* **2011**, *334*, 75.

[46] H. Kim, M. Seo, M.-H. Park, J. Cho, *Angew. Chem Int. Ed.* **2010**, *49*, 2146.

[47] J. Saint, M. Morcrette, D. Larcher, L. Laffont, S. Beatie, J.-P. Pérès, D. Talaga, M. Couzi, J.-M. Tarascon, *Adv. Funct. Mater.* **2007**, *17*, 1765.

[48] X. Huang, J. Yang, S. Mao, J. Chang, P. B. Hallac, C. R. Fell, B. Metz, J. Jiang, P. T. Hurley, J. Chen, *Adv. Mater.* **2014**, *26*, 4326.

[49] Y. Gogotsi, P. Simon, *Science* **2011**, *334*, 917.

[50] M. J. Grau, O. Kayser, R. H. Müller, *Int. J. Pharm.* **2000**, *196*, 155.

[51] S. D. Beattie, D. Larcher, M. Morcrette, B. Simon, J.-M. Tarascon, *J. Electrochem. Soc.* **2008**, *155*, A158.

[52] B. Wang, X. Li, T. Qiu, B. Luo, J. Ning, J. Li, X. Zhang, M. Liang, L. Zhi, *Nano Lett.* **2013**, *13*, 5578.

[53] S. Xun, B. Xiang, A. Minor, V. Battaglia, G. Liu, *J. Electrochem. Soc.* **2013**, *160*, A1380.

[54] J. Song, J. Zhou, R. Yi, T. Xu, M. Gordin, D. Tang, Z. Yu, M. Regula, D. Wang, *Adv. Funct. Mater.* **2014**, *24*, 5904.